Collision-enhanced Hanle resonances and transverse optical pumping in four-wave light mixing in Na vapor

Y. H. Zou* and N. Bloembergen
Division of Applied Sciences, Harvard University, Cambridge, Massachusetts 02138
(Received 23 September 1985)

Collision-enhanced Hanle resonances in the $3\,^2S_{1/2}$ electronic ground state of Na atoms have been studied in a phase-conjugate four-wave light-mixing geometry. Narrow resonances in zero magnetic field have been observed at very high inert-buffer-gas pressures, with a width of 21 mG, or less than 10 kHz, full width at half-maximum. The intensity and the width of these resonances has been studied as a function of buffer-gas pressure, of alkali-metal vapor pressure, of detuning from the D_1 and D_2 Na resonances, and of the intensity of the incident light beams. Saturation phenomena and power broadening are observed. The results are explained theoretically in terms of transversely pumped optical gratings. The equivalence of this description with collision-induced coherence gratings in the limit of low light intensities is demonstrated.

I. INTRODUCTION

The historical background of collision-induced coherences in four-wave light mixing has been outlined in a previous paper by Rothberg and Bloembergen.[1] That paper will henceforth be referred to as I, and the present paper may be considered as a logical extension of those earlier studies. In particular, the Zeeman coherences are now studied in the limit of zero external magnetic field, in which case the Zeeman levels become degenerate. In this case collision-induced degenerate frequency resonances are observed, which may quite properly be designated as collision-enhanced Hanle resonances.[2] The purpose of this paper is to present detailed investigations of these Hanle-type four-wave-mixing resonances as a function of intensity of the incident light beams, as a function of the detuning Δ of the incident frequency from the D_1 and D_2 resonance lines in Na vapor, and as a function of alkali-metal vapor pressure and buffer-gas pressure.

A. Brief review of collision-enhanced Zeeman coherence

Consider an atomic system in the electron ground-state configuration with Zeeman sublevels $|g\rangle, |g'\rangle, |g''\rangle, \ldots$. Since the Zeeman splitting is small compared to kT, the initial population of each of these levels is the same, $\rho^{(0)}_{gg}=\rho^{(0)}_{g'g'}=\rho^{(0)}_{g''g''},\ldots$. An excited electronic state has Zeeman sublevels $|n\rangle, |n'\rangle, |n''\rangle,\ldots$. These levels are initially unoccupied, $\rho^{(0)}_{nn}=\rho^{(0)}_{n'n'}=\rho^{(0)}_{n''n''}=0$. Now this atomic system is subjected simultaneously to two incident light beams,

$$E=\tfrac{1}{2}E_1\hat{\mathbf{z}}e^{i\mathbf{k}_1\cdot\mathbf{r}-i\omega_1 t}+\tfrac{1}{2}E_2\hat{\mathbf{y}}e^{i\mathbf{k}_2\cdot\mathbf{r}-i\omega_2 t}+\text{c.c.}\ . \tag{1}$$

In the impact approximation the density-matrix equations of motion are augmented by phenomenological damping terms of the Bloch type. Standard second-order perturbation theory leads immediately to a Zeeman coherence in the ground-state manifold:[1]

$$\rho^{(2)}_{gg'}(\omega_1-\omega_2)=\sum_n \frac{\mu_{ng}\mu_{g'n}E_1E_2^*}{4\hbar^2[\omega_{g'g}-(\omega_1-\omega_2)+(\mathbf{k}_1-\mathbf{k}_2)\cdot\langle\mathbf{v}_{\rm th}\rangle-i\Gamma_{g'g}]} \times\left[\frac{\rho^{(0)}_{gg}}{\omega_1-\omega_{ng}-\mathbf{k}_1\cdot\langle\mathbf{v}_{\rm th}\rangle-i\Gamma_{ng}}+\frac{\rho^{(0)}_{g'g'}}{\omega_{ng'}-\omega_2+\mathbf{k}_2\cdot\langle\mathbf{v}_{\rm th}\rangle-i\Gamma_{ng'}}\right]\exp[i(\mathbf{k}_1-\mathbf{k}_2)\cdot\mathbf{r}-i(\omega_1-\omega_2)t]\ . \tag{2}$$

Here μ_{ng} and $\mu_{g'n}$ are the electric dipole matrix elements connecting the ground Zeeman states $|g\rangle$ and $|g'\rangle$ with the excited states $|n\rangle$. The Doppler shifts for one-photon processes are $\mathbf{k}_1\cdot\langle\mathbf{v}_{\rm th}\rangle$ and $\mathbf{k}_2\cdot\langle\mathbf{v}_{\rm th}\rangle$, while the Doppler shift for a Raman-type process between the two Zeeman sublevels is $(\mathbf{k}_1-\mathbf{k}_2)\cdot\langle\mathbf{v}_{\rm th}\rangle$. A suitable average over the thermal velocities of the atoms has to be taken. In the limit of high buffer-gas pressures, this average becomes a diffusive drift velocity. The Zeeman splitting is $\omega_{g'g}=\hbar^{-1}g\beta B_0$, where B_0 is an external magnetic field which lifts the degeneracy of the Zeeman levels. The collision-induced phenomena become prevalent for sufficiently large detuning from the one-photon resonances $\Delta\gg\omega_1-\omega_2,\mathbf{k}_1\cdot\langle\mathbf{v}_{\rm th}\rangle,\Gamma_{ng}$. Near the Raman-type resonance $\omega_1-\omega_2=\omega_{g'g'}$ one has $\Delta=\omega_1-\omega_{ng}=\omega_2-\omega_{ng'}$. With the one-photon resonance width being the same for all sublevels, $\Gamma_{ng}=\Gamma_{ng'}=\Gamma$, Eq. (2) reduces to

$$\rho^{(2)}_{gg'}=\frac{\mu_{ng}\mu_{g'n}E_1E_2^*}{4\hbar^2[\hbar^{-1}g\beta B_0-(\omega_1-\omega_2)+(\mathbf{k}_1-\mathbf{k}_2)\cdot\langle\mathbf{v}_{\rm th}\rangle-i\Gamma_{g'g}]} \times\left[\frac{\Delta(\rho^{(0)}_{g'g'}-\rho^{(0)}_{gg})}{\Delta^2+\Gamma^2}-\frac{i\Gamma(\rho^{(0)}_{g'g'}+\rho^{(0)}_{gg})}{\Delta^2+\Gamma^2}\right]\exp[i(\mathbf{k}_1-\mathbf{k}_2)\cdot\mathbf{r}-i(\omega_1-\omega_2)t]\ . \tag{3}$$

The first term in the square brackets is the conventional Raman coherence, which vanishes for equal initial population of the Zeeman sublevels. The second term is proportional to the sum of the populations in the two levels but also proportional to the damping constant Γ, for $\Delta \gg \Gamma$. This constant is considerably enhanced by the presence of collisions

$$\Gamma = \tfrac{1}{2} t_{\rm sp}^{-1} + c_0 p \ . \tag{4}$$

The first term on the right-hand side of Eq. (4) represents the natural width due to spontaneous emission from level $|n\rangle$, the second term is proportional to the buffer-gas pressure p, with c_0 being a constant. The cross section for state-changing collisions in the $3\,^2P$ manifold is about 3×10^{-14} cm^2 for Na-Ar collisions.[3] The second-order coherence can be increased by many orders of magnitude by such collisions. Note that the width of the Raman-type resonance between Zeeman levels in the ground-state manifold is independent of the lifetime of the excited states.

For alkali-metal vapors in an inert noble buffer gas $\Gamma_{gg'}$ may lie in the kilohertz range, even for many atmospheres of buffer-gas pressure,

$$\Gamma_{gg'} = c_2 p + f(p_{\rm Na}) \ . \tag{5}$$

The constant c_2 is many orders of magnitude smaller than c_0, as collisions between a noble-gas atom and an alkali-metal atom in the $3\,^2S$ ground-state configuration are very ineffective in flipping the electron spin. A cross section for this process of 8.8×10^{-23} cm^2 for Na-Ar collisions and 2.5×10^{-20} cm^2 for Na-Xe collisions has been obtained from optical-pumping experiments.[4,5]

The contribution of spin-exchange Na-Na collisions to the width $\Gamma_{gg'}$ presents a very interesting problem, which has been discussed in detail by Happer *et al.*[6] In the experiments to be described in this paper, the contribution $f(p_{\rm Na})$ from spin-exchange collisions is always smaller than 3 kHz. A further discussion of this term will be postponed until Sec. III.

The influence of the buffer-gas pressure on the inhomogeneous broadening is also remarkable. The Doppler broadening of the Raman-type resonance given by the first factor in the denominator on the right-hand side of Eqs. (2) and (3) is proportional to

$$\Delta\omega_{\rm res,D} = (\mathbf{k}_1 - \mathbf{k}_2)\cdot\langle \mathbf{v}_{\rm th}\rangle \approx |k_1|\,\theta^2 (kT/M)\tau_c \ . \tag{6}$$

Here θ is the small angle between the wave vectors $\mathbf{k}_1$ and $\mathbf{k}_2$, which are of equal length, and τ_c is the time between the collisions of a Na atom with the buffer gas. More precisely, it is the correlation time of the thermal atomic velocity component parallel to $\mathbf{k}_1 - \mathbf{k}_2$. The mean square of this velocity component is kT/M, where M is the mass of the Na atom (or, more precisely, the reduced mass in Na—buffer-gas-atom collisions). Equation (6), which is valid in the limit $\tau_c\,|(\mathbf{k}_1-\mathbf{k}_2)\cdot\mathbf{v}_{\rm th}| \ll 1$, may be understood as a collisional averaging of the instantaneous Doppler shift $|(\mathbf{k}_1-\mathbf{k}_2)\cdot\mathbf{v}_{\rm th}|$. As the velocity component in the direction of the coherence grating rapidly changes, the instantaneous Doppler shift changes sign many times in a time interval which is equal to the inverse of the instantaneous Doppler shift. This Dicke-type averaging[7] is entirely analogous to the motional narrowing of magnetic resonance lines by averaging over the instantaneous values of the internal local magnetic fields.[8] The same situation can be described equally well in the spatial domain as in the time domain. When the mean-free path of the Na atoms $l \approx |\mathbf{v}_{\rm th}|\,\tau_c$ is small compared to the coherence grating constant $|\mathbf{k}_1 - \mathbf{k}_2|^{-1}$, the washing out of the grating occurs in the time it takes a Na atom to diffuse over one grating constant. The inverse of this time is again given by the right-hand side of Eq. (6). We thus find that the inhomogeneous contribution to the width is proportional to τ_c, or inversely proportional to the buffer-gas pressure p. Thus high-buffer-gas pressures are advantageous in two ways. The magnitude of coherence is increased as it is proportional to Γ/Δ^2, according to Eq. (3), and the inhomogeneous width is decreased. This situation is rather specific for the alkali vapors with noble-gas buffers. If the ground state of the atom is not a very pure S state, the collisions may contribute substantially to the homogeneous width $\Gamma_{gg'}$, corresponding to a larger constant c_2 in Eq. (5).

Second-order perturbation theory also yields a Zeeman coherence induced in the excited state $\rho^{(2)}_{nn'}$. The homogeneous width of this resonance $\Gamma_{nn'} \approx \Gamma_{ng} + \Gamma_{n'g}$ will, however, be very broad, with the broadening increasing with increasing buffer-gas presure. Excited-state coherences were first observed by Prior *et al.*,[9] and Zeeman coherences in the excited state were first discussed by Grynberg.[10]

B. Brief review of experimental Hanle resonances in four-wave light mixing

The existence of the second-order coherence grating given by Eq. (3) may be demonstrated by the diffraction of a third-incident light beam with wave vector $\mathbf{k}_3$ and frequency ω_3. The intensity of a new fourth wave with wave vector $\mathbf{k}_4$ and frequency ω_4 will be large, if the conditions of energy and momentum conservation can be simultaneously satisfied, $\omega_4 = \omega_1 - \omega_2 + \omega_3$ and $\mathbf{k}_4 = \mathbf{k}_1 - \mathbf{k}_2 + \mathbf{k}_3$. For $|\omega_1 - \omega_2| \ll \omega_1$ and $|\Delta\mathbf{k}| = |\mathbf{k}_1 - \mathbf{k}_2| \ll |\mathbf{k}_1|$ and $|\mathbf{k}_2|$, a three-dimensional near-forward scattering geometry is generally useful, as discussed in I and references quoted therein. The resonance in the intensity of the fourth beam may be scanned as ω_2, and therefore $\omega_1 - \omega_2$ is varied at fixed B_0, or B_0 may be varied as ω_1 and ω_2 are kept fixed.

As the external magnetic field is reduced to zero, the Zeeman levels become degenerate. A frequency-degenerate resonance occurs for $\omega_1 = \omega_2$, as Eqs. (2) and (3) retain their validity in the limit $B_0 \to 0$. In this case one may choose $\omega_1 = \omega_2 = \omega_3$. The three light beams may be derived from a single, frequency-stabilized dye laser. It now also becomes advantageous to choose $\mathbf{k}_3 = -\mathbf{k}_1$, so that the fourth beam corresponds to the phase-conjugate reflected wave with $\mathbf{k}_4 = -\mathbf{k}_2$. The resonance in the Zeeman coherence now occurs at $B_0 = 0$. This zero-field level-crossing resonance may appropriately be designated as a Hanle-type resonance. The Hanle effect of the polarization properties of resonance fluorescence as a function

of a weak external magnetic field is based precisely on this type of coherence between crossing energy levels. In the four-wave mixing experiment the coherence grating becomes stationary, independent of time, for $\omega_1=\omega_2$.

The first Hanle-type experiments in four-wave mixing were carried out by Scholz *et al.*[11] in ytterbium with argon-buffer gas. Following the suggestion of Grynberg,[10] they observed the Zeeman coherence in the excited electronic configuration. In agreement with the discussion of Sec. I A, the resonances were broad, tens to hundreds of gauss, and the width increased rapidly with increasing buffer-gas pressure.

We have briefly reported the observation of a Hanle-type resonance with a width of 35 mG,[2] due to Zeeman coherence in the $3\,^2S_{1/2}$ ground-state configuration of Na atoms. Presented in this paper are the results of a systematic investigation on the intensity and width of this sharp resonance as a function of several parameters. The detuning $\Delta=\omega_1-\omega_{ng}$, where ω_{ng} is either the D_1 or D_2 resonant frequency, the buffer-gas pressure p, and the intensity of the incident light beams $|E_1|^2$ and $|E_2|^2$ were systematically varied over intervals of several orders of magnitude. Data were also taken at different pressures of alkali-metal vapor. In Sec. II the experimental method is described. In Sec. III the experimental results in the limit of low-incident light intensity are presented and compared with perturbation theory. In Sec. IV it is shown that an equally valid description of these collision-induced Zeeman coherences may be given in terms of collision-enhanced transverse optical pumping. The optical-pumping language is readily extended to retain validity at higher light intensities. The experimental data at these higher intensities, which include saturation phenomena and power broadening, are presented in Sec. V, although they historically preceded the theoretical discussion in Sec. IV. In the final section, VI, a summary of the most important conclusions is given.

II. EXPERIMENTAL METHOD

The experimental configuration is schematized in Fig. 1. The sodium vapor, which provides the optical nonlinearity, is generated in a heat pipe oven. A copper versus constantan thermocouple, fixed on the outside surface of the oven tube at the center, is used to measure the temperature, which determines the alkali-metal vapor pressure. Unfortunately, the temperature of the sodium supplied in the heat pipe may be somewhat lower. We use the following nominal values $p_{Na}=1.24\times10^{-5}$ torr for a reading $T=160$°C, $p_{Na}=2.7\times10^{-3}$ torr for $T=260$°C, and $p_{Na}=1.09\times10^{-2}$ torr for $T=294$°C. A gas-handling system was designed to add buffer gas (He, Ne, Ar, Xe, or N_2) with pressures ranging from 10 torr up to 23 000 torr, or from about 10^{-2} to 30 atm. The pressure is measured by a capacitance manometer (MKS baratron type 170 M-26B) or a high-pressure gauge at oven temperature.

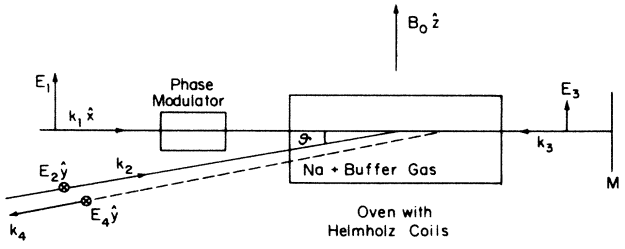

FIG. 1. Geometry of the four-wave mixing experiment with collision-enhanced Hanle resonances.

The stray and earth's magnetic field is canceled in two directions by sets of Helmholtz coils. In the remaining direction, taken as the z axis, a third set of Helmholtz coils is used to linearly scan the field through zero field. Any magnetizable material is avoided in the oven or in the vicinity of the Helmholtz coils to obtain a field inhomogeneity smaller than 8 mG over the interaction volume. Because the magnetic field due to the environmental currents changes occasionally, the balancing currents in the coils are checked frequently.

A typical phase-conjugation geometry is used for four-wave light mixing. All three incident beams are driven from a single-mode, frequency-stabilized dye laser (Coherent 599-21), which is pumped by an argon laser (Spectra Physics Model 171-19, at 514 nm). The output of the dye laser is monitored with a spectrum analyzer (Tropel Mode 240). A 10-GHz free-spectral-range Fabry-Perot etalon is used to measure the detuning of the dye laser from the D_1 or D_2 resonance. The detuning could be varied over about 10^3 GHz, or 30 cm^{-1}.

The geometry of the light beams is shown in Fig. 1. The light beam $\mathbf{k}_1$ propagates at right angles to the varying magnetic field. This direction is taken as the x direction. This beam is linearly polarized parallel to $B_0\hat{z}$. The beam with wave vector $\mathbf{k}_2$ is derived by means of a beam splitter. The angle θ between $\mathbf{k}_1$ and $\mathbf{k}_2$ could be varied between 0.3° and 1.5° or 5×10^{-3}–2.5×10^{-2} rad. The beams were focused into the interaction region at the center of the heat pipe by a common lens. Focal lengths of 20 and 35 cm were used. In most experiments the amplitudes of the two beams, $|E_1|$ and $|E_2|$, were about equal. The Gaussian profile of the beams was carefully measured at the output of the dye laser, so that the spot size in the oven could be calculated reliably. The linear polarization of the second beam was orthogonal to that of $\mathbf{k}_1$ by passage through a double Fresnel-rhomb half-wave retarder. The polarization of the second beam is consequently in the y direction. The two beams lead to a Zeeman coherence $\rho^{(2)}_{mm'}$ between adjacent Zeeman levels, with selection rule $\Delta m=m'-m=\pm1$, as discussed in I.

This coherence is probed by a beam with wave vector $\mathbf{k}_3=-\mathbf{k}_1$, propagating in the negative x direction. This beam is obtained by a mirror M, reflecting the beam $\mathbf{k}_1$ emerging from the oven back onto itself. In some experiments care was taken to make the probe-beam intensity small compared to the intensities of the first two beams $|E_3|\ll|E_1|=|E_2|$. This was accomplished by means of a filter in front of the mirror. The polarization of the backward probe beam is in the z direction. The four-wave mixing signal with wave vector $\mathbf{k}_4=-\mathbf{k}_2$ is split off by means of a 50% beam splitter. It is polarized

in the y direction. The spatially filtered signal, after passage through a polarizer to discriminate against z-polarized scattered light from the $\mathbf{k}_3$ beam, is detected by a photomultiplier tube operated in the linear regime of low gain. Additional discrimination against scattered light from the $\mathbf{k}_1$ and $\mathbf{k}_2$ beams is provided by a mechanical chopper, which modulates the probe beam $\mathbf{k}_3$. The resulting modulation in the phase-conjugate signal is synchronously detected by a Princeton Applied Research HR-8 lock-in amplifier.

The beam $\mathbf{k}_1$ can be phase modulated by a quantum technology model XPZ-B1-P modulator. This provides side bands with frequency components $\omega \pm n\omega_m$ in this beam. The signal intensity in an experimental run with $\omega_m = 620$ kHz as a function of B_0 is shown in Fig. 2. The modulation depth was such that the power in beam $\mathbf{k}_1$ at ω was 1.4 mW, the power in the side bands at $\omega \pm \omega_m$ was 2 mW, and the power in the side bands at $\omega \pm 2\omega_m$ was 0.5 mW. The focal spot size has an area of about 3×10^{-4} cm^2. The detuning $\Delta = 55$ GHz below the $^2P_{1/2}$ or D_1 resonance was used. The partial pressure of the helium buffer gas was 2010 torr. The angle $\theta \approx 1°$.

Figure 2 demonstrates the existence of a Zeeman resonance when $\hbar\omega_m = g\beta B_0$ and $2\hbar\omega_m = g\beta B_0$. These resonances occur at $B_0 = 0.89$ G and $B_0 = 1.78$ G, respectively. It should be noted that the full width at half-maximum (FWHM) width of these resonances is roughly 0.47 G or about 330 kHz. This is more than one order of magnitude narrower than the narrowest width obtained in I. In this earlier work two independently tunable dye lasers were used, and it was, correctly, surmised that the observed width was instrumental in origin and caused by the relative frequency fluctuations in the two lasers. In the present experiment with a single laser, such frequency fluctuations in the difference frequency $\omega_1 - \omega_2$ are eliminated. Figure 2 also reveals a Hanle resonance for $B_0 = 0$. A saturation dip appears in the center of this resonance.

Significantly narrower resonances than those exhibited in Fig. 2 can be obtained by taking a number of steps. The Doppler broadening given by Eq. (6) is reduced further by choosing a smaller value of the angle θ and a higher buffer-gas pressure. Power broadening and saturation effects may be eliminated by reducing the beam intensities. The results of perturbation theory, expressed in Eqs. (2) and (3), are strictly valid in the weak-field limit defined by

$$\frac{\Omega_1^2 \Gamma}{\Delta^2 + \Gamma^2} \ll \Gamma_{gg'} \tag{7}$$

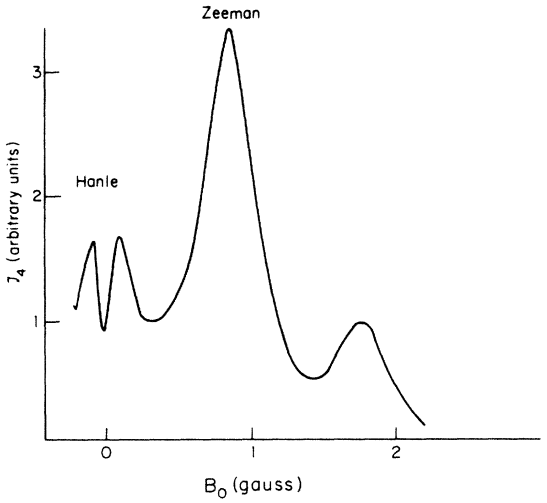

FIG. 2. Hanle resonance and Zeeman coherence in phase-conjugate four-wave light mixing with a phase modulation of 620 kHz on the beam $\mathbf{k}_1$. ($\theta = 1°$, $T_{\text{oven}} = 294$ °C, $\Delta = 55$ GHz below $^2P_{1/2}$, 2010 torr He.)

and

$$\frac{\Omega_2^2 \Gamma}{\Delta^2 + \Gamma^2} \ll \Gamma_{gg'} .$$

Here $\Omega_1 = \frac{1}{2}\hbar^{-1} |\mu_{ng}| |E_1|$ and $\Omega_2 = \frac{1}{2}\hbar^{-1} |\mu_{ng'}| |E_2|$ are the Rabi frequencies. These inequalities express the fact that the pumping-out rates from the ground states $|g\rangle$ and $|g'\rangle$ to the $3\,^2P$ manifold should be small compared to the relaxation rate $\Gamma_{gg'}$, reestablishing equilibrium in the ground-state manifold. The inequalities (7) imply, furthermore, that the second-order Rabi frequency, corresponding to Raman-type two-photon transitions between $|g\rangle$ and $|g'\rangle$, is also small,

$$\frac{\Omega_1 \Omega_2 \Gamma}{\Delta^2 + \Gamma^2} \ll \Gamma_{gg'} . \tag{7a}$$

It will be shown in more detail in Sec. IV that under these conditions power-broadening and saturation effects are negligible. The intensity of the phase-conjugate signal is proportional to the absolute square of the third-order susceptibility $|\chi^{(3)}|^2$. The quantity $\chi^{(3)}$ is proportional to the second-order coherence $\rho_{gg'}^{(2)}$ and to the response of the weak-signal beam $(\Delta - i\Gamma)^{-1}$. One thus finds

$$I_4 \propto \left| \frac{N_0(-i\Gamma)}{\hbar^3(\Delta - i\Gamma)(\Delta^2 + \Gamma^2)} \int_{-\infty}^{+\infty} \frac{\mu_{gn}\mu_{ng'}\mu_{g'n}\mu_{ng}}{\hbar^{-1} g\beta B_0 - (\omega_1 - \omega_2) + (\mathbf{k}_1 - \mathbf{k}_2)\cdot\langle \mathbf{v}_{\text{th}} \rangle - i\Gamma_{g'g}} f\langle \mathbf{v}_{\text{th}} \rangle d\langle \mathbf{v}_{\text{th}} \rangle \right|^2 |E_1|^2 |E_2|^2 |E_3|^2 . \tag{8}$$

In Fig. 3 a very narrow collision-enhanced Hanle resonance is reproduced with a FWHM width of 21 mG. In this case no phase modulation was imposed on beam $\mathbf{k}_1$. The intensity of the beams in the interaction region was reduced to 0.1 W/cm^2. The angle θ was reduced to 0.3°, and the buffer-gas pressure of argon was increased to $p = 8400$ torr. The detuning $\Delta = 50$ GHz below the D_1 resonance. Under these conditions the inequality [Eq. (7)]

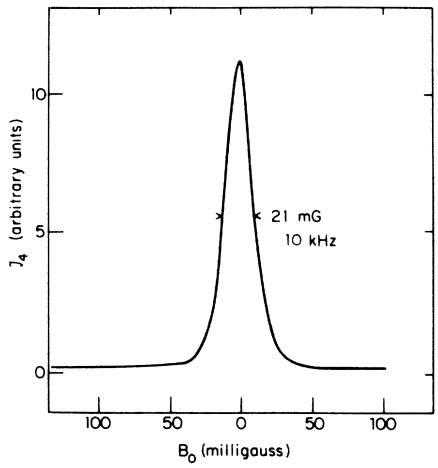

FIG. 3. Hanle resonance in phase-conjugate four-wave light mixing ($\theta=0.3°$, $T_{\text{oven}}=294°C$, $\Delta=50$ GHz below $^2P_{1/2}$, 8400 torr Ar, and $I_1=I_2=0.1$ W/cm^2).

is satisfied and $f\langle v_{\text{th}}\rangle$ in Eq. (8) may be replaced by a δ function.

In Sec. III we shall present the variation of the intensity and the width of the Hanle resonance in the weak-field limit, defined by Eq. (7), as a function of various parameters.

III. EXPERIMENTAL RESULTS IN THE WEAK-FIELD LIMIT

A. Linewidth

The FHWM linewidth as a function of argon-buffer-gas pressure is shown in a double logarithmic plot in Fig. 4. The width is inversely proportional to p up to $p=2000$ torr. This is in agreement with Eq. (6). The residual Doppler broadening at $\theta=0.3°$ decreases from 10 MHz at 3 torr to 10 kHz at 3000 torr (4 atm). The effect of finite interaction time due to diffusion out of the interaction region has the same pressure dependence as the Doppler broadening. For $\theta=0.3°$, the focusing of the beams may leave a coherence grating with only five fringes. Thus the effect of finite interaction area is a fraction of 20% or less of the Doppler contribution to the width. Velocity-changing collisions occur at a rate $N\bar{v}\sigma$. Each strong collision is effective in changing the $3\,^2P$ states. This makes a contribution $c_0 p$ to the width Γ_{ng}. For Na-Ar collisions this corresponds to a contribution to FWHM of $\Delta\nu=N\bar{v}\sigma/\pi=16$ MHz/torr. The constant c_2 in Eq. (5) corresponds to 4.3×10^{-2} Hz/torr. Thus, a broadening of the linewidth by this mechanism remains unobservable at the highest argon pressure used ($p=2\times10^4$ torr, or about 30 atm).

The conversion of the linewidth from frequency units to milligauss obviously involves the g value of the spin precession frequency. The g_F values in the $F=2$ and $F=1$ ground-state hyperfine levels of Na are $+\frac{1}{2}$ and $-\frac{1}{2}$, respectively. Happer[5,6] has pointed out that in the limit of small Zeeman splitting and high Na densities, when the spin-exchange collision rate is larger than the spin precession frequencies, an effective g value must be used. For a nuclear spin $I=\frac{3}{2}$, this value is $\frac{2}{3}g_F$. Thus the observed width of 21 mG corresponds to about 10 kHz. One should keep in mind that this correction factor of $\frac{2}{3}$ is only valid below $|B_0|<20$ mG for a Na vapor pressure of 10^{-2} torr. It does not apply to the Zeeman resonance frequency in an external field larger than 0.5 G, shown in Fig. 2. It also does not apply to the conversion to kHz of the linewidth data in Figs. 6 and 19. The primary experimental data are obtained in milligauss, and Happer's papers[5,6] have been used for the correct conversion to a frequency scale.

It is clear that at $p_{\text{Ar}}>10^4$ torr, the residual Doppler broadening is less than 3 kHz or 6 mG. The spin-changing Na-Ar collisions contribute 4.3×10^{-2} Hz/torr to the FWHM. This follows from $\Delta\nu=N\sigma\bar{v}/\pi$, with $\bar{v}=9.03\times10^4$ cm/s for Na-Ar collisions at 294°C, where σ is the cross section mentioned after Eq. (5). At $p_{\text{Ar}}=30$ atm, this contribution to $\Gamma_{gg'}$ is still smaller than 1 kHz. An attempt was made to experimentally determine the contribution $f(p_{\text{Na}})$ of spin-exchange Na-Na collisions to the homogeneous width $\Gamma_{gg'}$. The Na vapor pressure was varied by changing the oven temperature. The results are shown in Fig. 5.

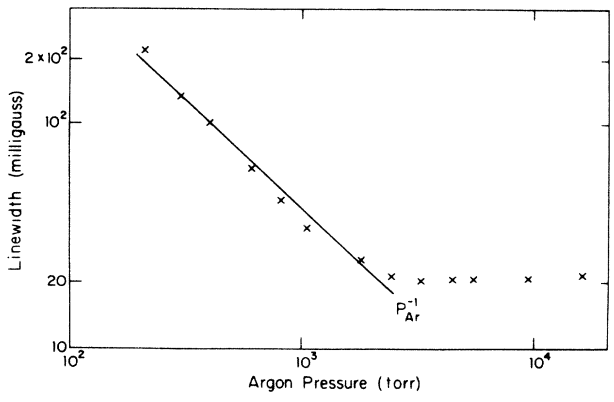

FIG. 4. Double logarithmic plot of the FWHM width of the collision-enhanced Hanle resonance versus argon-buffer-gas pressure. ($\theta=0.3°$, $T_{\text{oven}}=294°C$, $\Delta=50$ GHz below $^2P_{1/2}$, and $I_1=I_2=0.1$ W/cm^2.)

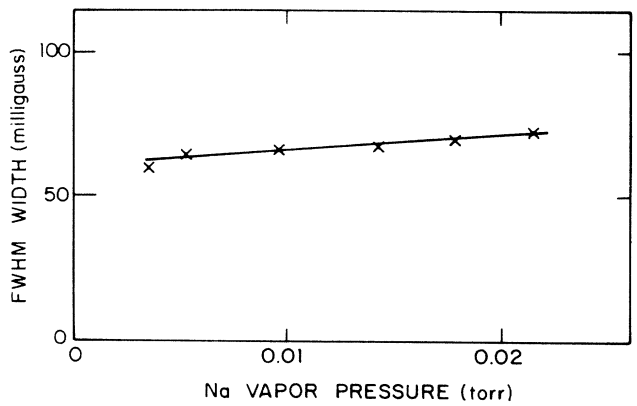

FIG. 5. Linewidth (FWHM) as a function of the Na vapor pressure. ($\theta=0.45°$, $\Delta=80$ GHz below $^2P_{1/2}$, 2050 torr Ar, and $I_1=0.2$ W/cm^2.)

If nuclear spin is ignored, one would not expect any contribution of spin-exchange collisions to the width of the Hanle resonance, as any component of the spin polarization commutes with the spin-exchange interaction. Thus the expectation value of the spin polarization remains unchanged and is not relaxed by such collisions. In the presence of nuclear spin, transitions between the hyperfine states $F=1$ and $F=2$ are induced by the spin-exchange collision. The Zeeman precession changes sign. The contribution to the width of the Zeeman resonance has been analyzed in detail by Happer.[5,6] In the limit $B_0 \rightarrow 0$ the contribution $f(p_{\mathrm{Na}})$ in Eq. (5) vanishes, according to his theory. If one takes an effective value $|B_0| \sim 10$ mG, corresponding to the half-maximum points, the rate of spin-exchange collisions at $p_{\mathrm{Na}}=10^{-2}$ torr is already faster than the effective precession frequency. One is therefore in the regime where the contribution to the linewidth would decrease with increasing vapor pressure, $f(p_{\mathrm{Na}}) \propto p_{\mathrm{Na}}^{-1}$. At $p_{\mathrm{Na}}=10^{-2}$ torr this contribution is calculated to be about 3 kHz from Happer's formulae. Although the data in Fig. 5 do not show a decrease of FWHM with increasing p_{Na}, they are nevertheless considered to be consistent with this theory, as the contribution to the observed width in the interval 0.5×10^{-2} torr $< p_{\mathrm{Na}} < 2\times10^{-2}$ torr is indeed less than 6 mG. In this context the following experimental difficulties should be noted. The observed signal intensity varies with p_{Na}^2, and the optical path length in the interaction region increases with p_{Na}. Therefore, the accuracy of the data in Fig. 5 is rather poor.

Since residual Doppler broadening and transit time effects, in combination with spin-changing collisions, cannot explain the observed asymptotic width of 10 kHz, two other instrumental causes must be taken into account. We have estimated the residual power broadening experimentally by increasing the intensities of the light beams. At the 0.1 W/cm^2 intensity, used in obtaining the data in Figs. 3 and 4, a residual contribution of about 4 mG or 2 kHz is estimated. The balance of the observed width of 10 kHz is caused by residual inhomogeneities in the magnetic field B_0 over the interaction region. These are estimated to amount to 8 mG or about 4 kHz. Improvement by reduction of this inhomogeneous broadening would require a complete redesign of the oven with μ-metal shielding. In summary, the observed width of 10 kHz in Fig. 4 consists of the following contributions: residual Doppler (3 kHz), spin-changing collisions (<2 kHz), residual power broadening (2 kHz), residual magnetic-field inhomogeneities (4 kHz).

We have also observed the linewidth in other buffer gases (He, Ne, Xe, and N_2). For the lighter gases the collision cross sections are smaller. Thus it takes a higher pressure of He or Ne to obtain the same Doppler narrowing as for Ar. The spin-changing cross section, expressed by the constant c_2 in Eq. (5), is also smaller. It is unobservable in our series of experiments. The constants c_0 and c_2 for the heavier buffer gas Xe are, however, considerably larger than for Ar. The observed linewidth as a function of Xe pressure is shown in Fig. 6. The increase in width above $p=2000$ torr is quite pronounced. The behavior of the width is well represented by an expression

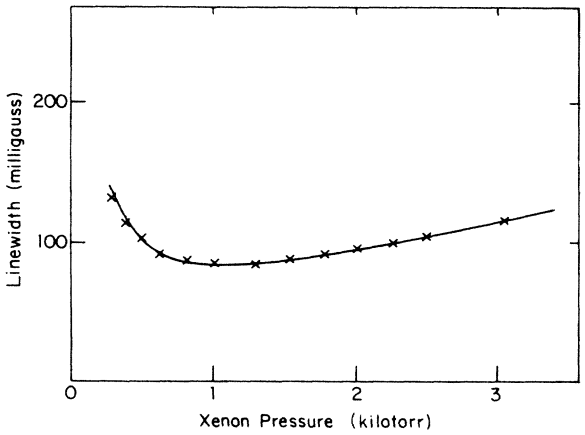

FIG. 6. The FWHM width of the collision-enhanced Hanle resonance versus xenon-buffer-gas pressure on a linear scale. ($\theta=0.3°$, $T_{\mathrm{oven}}=300$°C, $\Delta=50$ GHz below $^2P_{1/2}$, and $I_1=0.2$ W/cm^2.)

of the form $c'p^{-1}+c''+c_2p$. The first term describes the Doppler narrowing, the constant c'' contains the contributions from residual inhomogeneities in B_0 and from power broadening. Note that the data in Fig. 6 are not taken under the same experimental conditions as those in Fig. 4, where c'' would be smaller. The constant c_2 for Xe may be determined from Fig. 6. It corresponds to a spin-changing collision cross section between Xe and Na in the $3\,^2S_{1/2}$ ground state of 4.1×10^{-20} cm^2. This value is in good agreement with the results from optical-pumping experiments.[4]

The situation about the width of the resonances may be summarized as follows. The Doppler broadening becomes negligible for sufficiently small angle θ and sufficiently high buffer-gas pressures. An intrinsic homogeneous linewidth due to spin-changing collisions has been obtained with Xe pressures exceeding 3000 torr. In other cases the width is caused by residual inhomogeneities in B_0 and by residual power broadening.

B. Intensity

The collision-enhanced nature of these resonances is dramatically illustrated by the dependence of the peak intensity of the Hanle resonance at $B_0=0$ as a function of the argon pressure p, shown in Fig. 7. Referring to Eq. (8), the peak signal intensity is proportional to $\Gamma^2/\Gamma_{gg'}^2$, if $\Delta \gg \Gamma$ and if the residual Doppler broadening is negligible. Since $\Gamma \propto p$ and $\Gamma_{gg'}$ is independent of p above argon pressures $p=10^3$ torr, the intensity should be proportional to p^2, as verified by the upper part of the curve in Fig. 7. For $p<10^3$ torr, the line shape is mostly determined by Doppler broadening. While the integrated intensity of the Hanle resonance is still proportional to Γ^2, and thus to p^2, the peak intensity is inversely proportional to the residual Doppler width. Since the latter has a p^{-1} dependence, the peak intensity now has a p^3 behavior. Note that the break in the logarithmic plots in Figs. 4 and 7 occurs at the same value of p.

Next the variation of intensity with detuning is considered. When the detuning Δ is kept large compared to

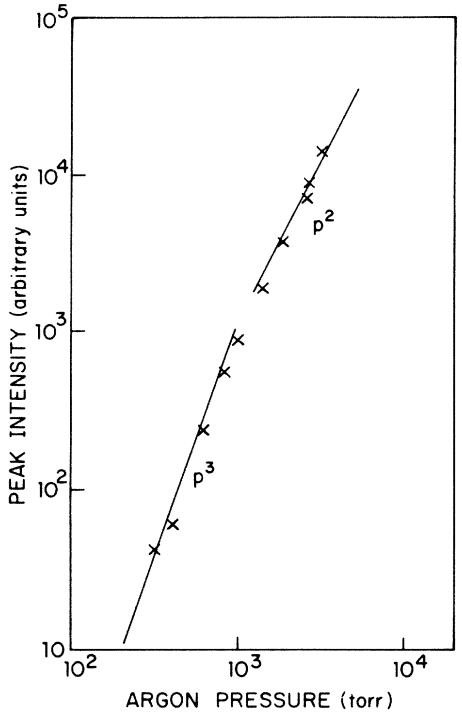

FIG. 7. Peak intensity of the collision-enhanced Hanle resonance versus argon-buffer-gas pressure. ($\theta=0.3°$, $T_{\text{oven}}=294\,°\text{C}$, $\Delta=50$ GHz below $^2P_{1/2}$, and $I_1=0.2$ W/cm^2.)

the one-photon Doppler broadening and to the one-photon collisional width, the attenuation of the light beams by one-photon absorption may be kept negligible. When Δ is also kept large compared to the hyperfine splitting of the ground-state manifold, amounting to 1.8 GHz, and is consequently also large compared to the splittings in the $3\,^2P_{1/2}$ and $3\,^2P_{3/2}$ manifolds, all nuclear-spin orientations are weighted equally. In this case the theoretical calculation may be restricted to the energy levels and the squared matrix elements, shown in Fig. 8, in which nuclear spin is ignored. The effects of nuclear spin on the effective g value and on spin-exchange broadening were discussed in Sec. III A in terms of Happer's theory. They do not change the integrated intensities.

With quantization in the z direction, the field E_{1z} produces a (virtual) transition without change of electron spin, the field E_{2y} produces a transition with $\Delta m=\pm 1$. Thus a Raman-type transition is induced between the

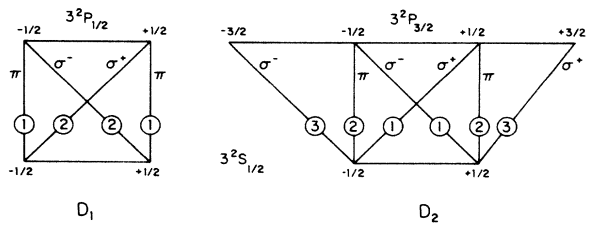

FIG. 8. The electronic energy levels and the relative transition rates for the D_1 and D_2 resonances of the Na atom.

$m_s=+\frac{1}{2}$ and the $m_s=-\frac{1}{2}$ level of the ground-state manifold. When the detuning Δ is kept small compared to the fine-structure splitting between the two P states, $\Delta \ll 17$ cm^{-1} or 500 GHz, either the contribution of the D_1 resonance dominates or the contribution of the D_2 resonance is dominant. Furthermore, for $\Delta \ll t_c^{-1}$, where $t_c < 10^{-12}$ s is the duration of a collision, the impact approximation should be valid. It is thus clear from Eq. (8) that in the range 20 GHz $<\Delta<$ 100 GHz, the intensity should vary as Δ^{-6}. This detuning behavior has been observed for detuning on both sides of the D_1 resonance, as shown in Fig. 9. The data were taken with an argon pressure $p=960$ torr and an oven temperature $T=250\,°\text{C}$. This collision-induced detuning behavior is also different from the contribution to the conventional Raman-type susceptibility, which is proportional to the population difference between the two levels. The right-hand sides of Eqs. (3) and (8) show that the conventional contribution, not enhanced by collisions, would lead to a Δ^{-4} dependence.

In order to investigate the behavior for large detunings, the oven temperature and the argon-buffer-gas pressure had to be increased to obtain an observable signal intensity for detunings out to 500 GHz, where $\Delta > t_c^{-1}$. Figure 10 shows the intensity of the Hanle resonance at $T=286\,°\text{C}$ and $p=4900$ torr for such larger detunings. There is a marked asymmetry. The intensity drops off much more rapidly on the high-frequency side than on the low-frequency side of the D_1 resonance.

Such asymmetric behavior was first observed by Scholz *et al.*[12] following a prediction by Grynberg[13] about the different behavior of collision-induced four-wave mixing outside the impact regime. An asymmetry of the resonance between two Zeeman states in the excited configu-

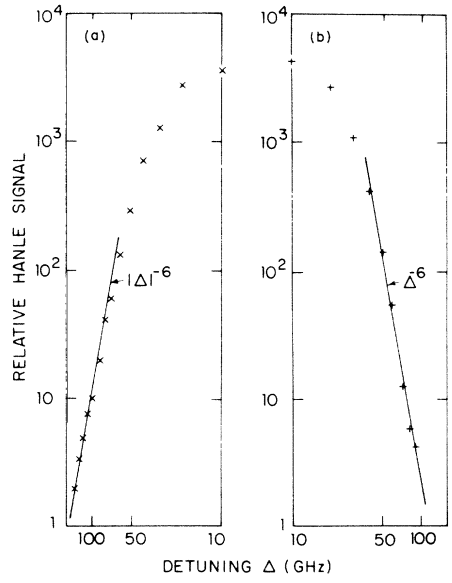

FIG. 9. Variation of peak Hanle signal intensity with detuning Δ: (a) below $^2P_{1/2}$; (b) above $^2P_{1/2}$. ($\theta=0.8°$, $T_{\text{oven}}=250\,°\text{C}$, 960 torr Ar, and $I_1=1.5$ W/cm^2.)

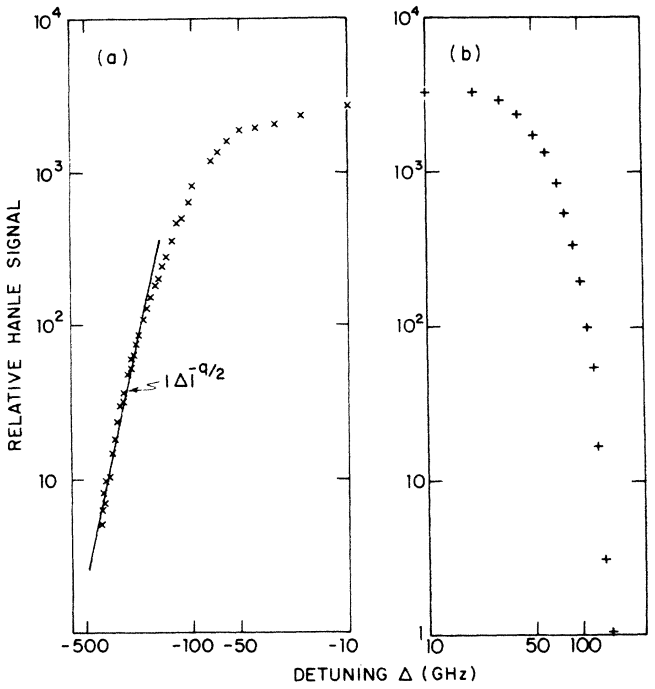

FIG. 10. Peak Hanle signal intensity for larger detuning Δ: (a) below $^2P_{1/2}$; (b) above $^2P_{1/2}$. ($\theta=0.8°$, $T_{oven}=286\,°C$, 4900 torr Ar, and $I_1=1.5$ W/cm^2.) Note the asymmetry due to breakdown of the impact approximation.

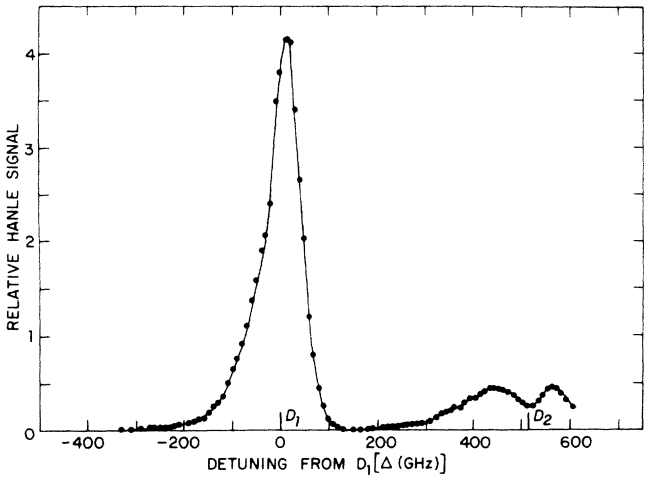

FIG. 11. Linear plot of peak intensity of the collision-induced Hanle resonances in the four-wave mixing signal versus laser frequency with saturation effects. ($\theta=0.8°$, $T_{oven}=265\,°C$, 4900 torr Ar, and $I_1=2$ W/cm^2.)

ration of Ba atoms with an argon-buffer gas was reported.[12]

The sharper resonances and higher intensities in the Na-atom ground state permit a better comparison between theory and experiment. Pressure-broadening theory in the wings for one-photon absorption is well developed.[14,15] For an attractive van der Waals potential between the colliding atoms, the cross section for one-photon processes with $\Delta \gg t_c^{-1}$ should drop off as $|\Delta|^{-3/2}$ on the red side (quasistatic wing). On the blue side (antistatic wing) the cross section should fall off as $\Delta^{-7/3}\exp(-\alpha\Delta^{5/6})$. Quite naively, one may expect the signal intensity for the frequency-degenerate four-wave light mixing to be proportional to the cube of the one-photon resonance response. This is born out by recent theoretical calculations by Prior *et al.*[16] Our experimental observations are consistent with a $|\Delta|^{-9/2}$ in the quasistatic wing and an exponential decrease in the antistatic wing.

A linear plot of the intensity variation over a wide range of Δ, at a fixed choice of the other parameters, $p=4900$ torr Ar, $T=265\,°C$, power level of 2 W/cm^2, is reproduced in Fig. 11. The difference in the vicinity of the D_1 and D_2 resonances is striking. Substitution of the relative matrix elements shown in Fig. 8 into the perturbation result, expressed by Eq. (8), leads immediately to the prediction of equal intensity for the same detuning from the D_1 and D_2 resonances, respectively. The breakdown of perturbation theory under the experimental conditions mentioned is evident. A deeper understanding of the different saturation behavior near the D_1 and D_2 resonances may be obtained by analyzing the Hanle resonances from a different point of view in a coordinate reference frame in which the axis of quantization is turned by 90°.

IV. COLLISION-ENHANCED TRANSVERSE OPTICAL PUMPING

At the center of the Hanle resonance the magnetic field $B_0\hat{\mathbf{z}}$ vanishes, and there is no compelling reason to choose the z axis as the axis of quantization. In fact, it would be more logical to choose the direction of propagation of the light beams, the x axis, as the preferred direction of spatial quantization. The coherence $\rho_{gg'}^{(2)}$ between Zeeman levels with z quantization corresponds to a magnetization in the plane perpendicular to $\hat{\mathbf{z}}$. This magnetization is static for $B_0=0$. When the x axis is chosen as the axis of quantization, this same magnetization would be described as a population difference between the two states with spin expectation values $s_x=+\frac{1}{2}$ and $s_x=-\frac{1}{2}$, respectively.

When the two linearly polarized beams in Eq. (1) have the same amplitude $|E_1|=|E_2|$, the relative phase of these beams varies as $\phi_1-\phi_2+(\mathbf{k}_1-\mathbf{k}_2)\cdot\mathbf{r}$. There are locations $\mathbf{r}$ where this phase difference equals $+90°$, and the light is right circularly polarized. For a displacement $\Delta\mathbf{r}$ with $(\mathbf{k}_1-\mathbf{k}_2)\cdot\Delta\mathbf{r}=\pi$, the light will be left circularly polarized. For $(\mathbf{k}_1-\mathbf{k}_2)\cdot\Delta\mathbf{r}=\pi/2$, a linear-light polarization results. Thus there exists in the Na vapor cell a polarization grating of light with grating constant $d=2\pi|\mathbf{k}_1-\mathbf{k}_2|^{-1}$. This grating, shown in Fig. 12, will produce a spin-orientation grating of the Na vapor by Kastler-type optical pumping.[17,18] Under the conditions of our experiments it is caused entirely by the fact that the $|+\rangle$ and $|-\rangle$ levels with x-directed quantization are pumped at different rates. Collisions are necessary to take up the detuning energy $\hbar\Delta$ for a transition to the P states.

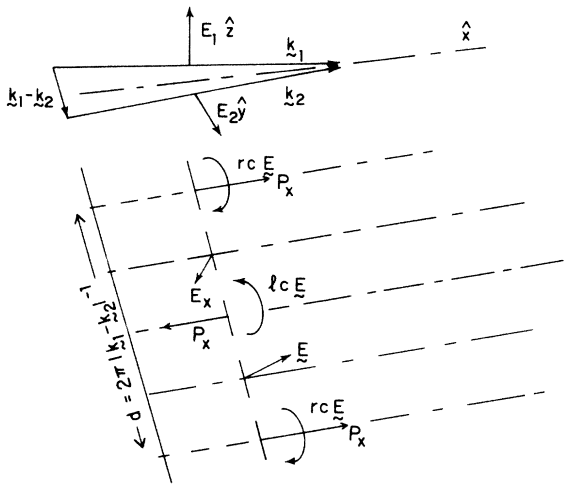

FIG. 12. Spin-orientation grating in ground state induced by Kastler-type pumping. rc is right circularly polarized light, lc left circularly polarized.

The same collisions produce a rapid equalization over all P levels. Subsequently, the P states decay by spontaneous emission, back to the ground-state configuration for $\Gamma \gg t_{\rm sp}^{-1}$. It is clear that the substates will all be refilled at the same average rate. Denote by N_+ the population in the $s_x=+\frac{1}{2}$ state. For σ^+-polarized light the pumping rate out of this level to the $^2P_{1/2}$ manifold is zero, $W_+=0$. The pumping rate from the $s_x=-\frac{1}{2}$ level is

$$W_- = \hbar^{-2}|\mu_{-,+}|^2 \frac{\Gamma}{\Delta^2+\Gamma^2}|E_{\rm rc}|^2 . \tag{9}$$

As long as the pumping-out rate is small compared to the spontaneous-emission rate, the population buildup in the P states remains negligible. This does not imply that this population is unobservable, since resonance fluorescence affords very sensitive detection. It does imply that the population-rate equations for the ground-state populations are simply given by

$$\frac{dN^+}{dt} = -W^+N^+ + \frac{W^+N^+ + W^-N^-}{2} - \Gamma_{g'g}(N^+ - N^-) + [-D\nabla^2(N^+ - N^-)] \tag{10}$$

and

$$\frac{dN^-}{dt} = -\frac{dN^+}{dt} .$$

These equations are an enormous simplification of the more general optical-pumping equations considered by Franzen,[19] Dehmelt,[20] and others. The sum of populations in the ground state remains constant $N^- + N^+ = N_0$. The first term on the right-hand side is the collision-assisted pump-out rate for the $s_x=+\frac{1}{2}$ level; the second term is the replenishing rate by spontaneous emission; the third term represents the effect of spin-changing collisions with the buffer gas in the ground-state manifold. Again, the effects of the spin-exchange collisions on the damping are ignored, which is, strictly speaking, incorrect for the nuclear spin $I=\frac{3}{2}$. The discussion in Sec. III has, however, demonstrated that such effects are small under the experimental conditions used. The last term in Eq. (10) represents the diffusional motion of the Na atoms, which tends to wash out the spin-orientation grating. The diffusion constant is $D \approx \frac{1}{3} v_{\rm th}^2 \tau_c \approx (kT/M)\tau_c$. One immediately finds the steady-state population difference for the x-directed eigenstates,

$$\Delta N = N^+ - N^- = \frac{W^- - W^+}{4(\Gamma_{gg'} + \Delta\omega_{\rm res,D}) + W^+ + W^-} N_0 , \tag{11}$$

where $\Gamma_{gg'}$ and $\Delta\omega_{\rm res,D}$ are given by Eqs. (5) and (6), respectively. The condition for the validity of the perturbation theory given by Eq. (7) is equivalent to the condition for weak optical pumping,

$$W^+ + W^- \ll 4(\Gamma_{gg'} + \omega_{\rm res,D}) . \tag{12}$$

Since the diffusion term is equivalent to an additional relaxation mechanism, it would be appropriate to add $\omega_{\rm res,D}$ also to the right-hand side of Eq. (7).

The x-directed population difference is proportional to the differential pumping rate $W^- - W^+$. The square of the matrix elements in Fig. 8 shows that this differential pumping rate is the same for pumping near the D_1 and the D_2 resonance, $|2-0| = |1-3|$. The x-directed magnetization grating has the same magnitude, but the opposite sign near the D_1 and the D_2 resonance. The sign is, however, not detectable in the four-wave-mixing experiment, which only measures the intensity of the grating. The intensity of the four-wave-mixing signal should be the same. Thus, it may be concluded that collision-enhanced Hanle effect is indeed identical to collision-assisted transverse optical pumping in the weak-pumping limit.

When a small external magnetic field B_0 is present, the ground-state-spin magnetization will start to process. After a time $t=\hbar\pi/g\beta B_0$, the magnetization will have switched from the $+x$ to the $-x$ direction. In order to be at the resonance for Zeeman coherence, the two beams with orthogonal linear polarization now have different frequencies $\hbar(\omega_1-\omega_2)=g\beta B_0$. Thus at a fixed point in space, $\mathbf{r}+\Delta\mathbf{r}$, the phase difference between the two light beams changes by π in the same time interval $\hbar\pi/g\beta B_0$. The sense of circular polarization switches from the right to left circular sense so as to keep the optical pumping going in the rotating frame of reference at a given location. This corresponds precisely to the configuration of dynamical optical pumping by modulated light beams, introduced by Bell and Bloom.[21]

The language of transverse optical pumping is especially advantageous to describe saturation effects which occur at strong optical pumping. This regime is defined by

$$\frac{1}{t_{\rm sp}} \gg W^+ + W^- \gg 4(\Gamma_{gg'} + \Delta\omega_{\rm res,D}) . \tag{13}$$

The inequality on the left ensures that the fraction of Na atoms in the excited configuration remains very small.

The inequality on the right-hand side takes into account that the x-directed magnetization at a fixed location may be changed not only by spin-changing collisions, but also by the diffusion of Na atoms from locations in the grating with a different magnetization. This relaxation mechanism was termed motion-induced lifetime shortening by Ducloy and Bloch.[22] This population-diffusion mechanism is incorporated in the rate equations (10).

In the regime of strong optical pumping, defined by Eq. (13), the population difference attains an asymptotic value. For pumping near the D_1 resonance, one has for purely circular polarized light, $W^+=0$,

$$\Delta N^{\rm as}(D_1)=N_0 \ .$$

Indeed, all the Na atoms are pumped to the $s_x=+\frac{1}{2}$ state. For pumping near the D_2 resonance, one finds with $W^-=\frac{1}{3}W^+$,

$$\Delta N^{\rm as}(D_2)=-\tfrac{1}{2}N_0 \ .$$

In this case, three-quarters of the Na atoms are in the $s_x=-\frac{1}{2}$ state and one-quarter are in the $s_x=+\frac{1}{2}$ state.

Under strong pumping near the D_1 resonance, the Na vapor is completely bleached. No further absorption of the pump light can take place in the steady state. This phenomenon has been termed "coherent population trapping" (Ref. 23). For pumping near the D_2 line, one-photon absorption can always occur. This may produce considerable attenuation of the light at the D_2 resonance and is responsible for the dip in the observed four-wave mixing signal displayed in Fig. 11. In the asymptotic regime of strong optical pumping, the population difference reaches an asymptotic value. It cannot be increased further, by either increasing the intensity of the pumping light, by reducing the detuning Δ or by increasing the buffer-gas pressure. Thus the dependence of the four-wave mixing signal on these parameters should be entirely different in this regime.

For strong optical pumping, power broadening of the Hanle resonance also becomes important. Numerous authors have given explicit solutions for a three- or four-level atomic system subjected to two electromagnetic waves of arbitrary amplitudes.[24,25] Orriols[26] has calculated the power broadening in the ground-state manifold of alkali-metal atoms and concluded that a broadening of the Zeeman or Hanle resonances sets in well before the saturation of the one-photon absorption resonances. It occurs precisely in the regime given by Eq. (13). The power broadening (FWHM) of the Hanle resonance is then simply given by

$$\Delta\omega_{\rm power}=\frac{2\Omega_1^2\Gamma}{\Delta^2+\Gamma^2}+\frac{2\Omega_2^2\Gamma}{\Delta^2+\Gamma^2} \ . \tag{14}$$

It may be interpreted as a shortening of the lifetime of the levels $|g\rangle$ and $|g'\rangle$, by the "pumping-out" rate from these levels. Thus power broadening sets in as soon as the second-order perturbation theory breaks down. If the third light beam, or probe beam, is not weak, it would also contribute a similar term to the power broadening.

The strong pumping regime, defined by the inequalities in Eq. (13), may be experimentally reached by raising the light intensity, by decreasing the detuning Δ, or by increasing the buffer-gas pressure, which increases Γ, for $\Delta \gg \Gamma$. In Sec. V experimental results in this regime are discussed.

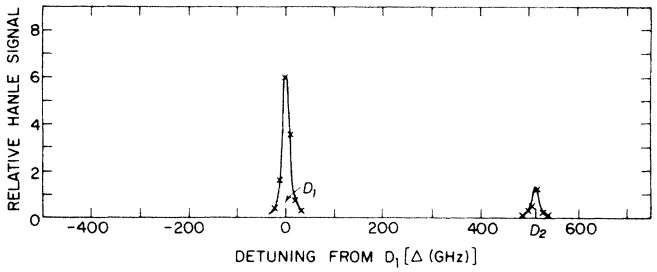

FIG. 13. Peak intensity of Hanle resonance with laser frequency at low-Na-vapor pressure, or low-optical density. ($\theta=0.5°$, $T_{\rm oven}=155\,°$C, 1000 torr Ar, and $I_1=I_2=0.5$ W/cm^2.)

V. EXPERIMENTAL RESULTS FOR STRONG PUMPING

Returning to the experimental data in Fig. 11, the very different behavior in the vicinity of the D_2 resonance can be understood by the strong optical-pumping behavior. While at the D_1 resonance the vapor becomes optically transparent due to complete bleaching, at the D_2 resonance the optical thickness of the vapor may remain significant. Optical attenuation causes the dip at the D_2 resonance. This was demonstrated experimentally by significantly lowering the Na vapor pressure in the cell. At an oven temperature $T=155\,°$C the response curves in Fig. 13 were obtained. The optical depth of a single beam at

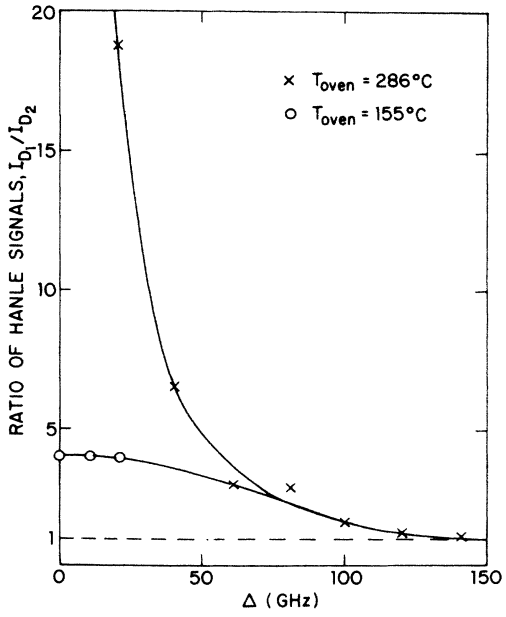

FIG. 14. The evolution from weak to strong optical pumping by reducing the detuning Δ. ($\theta=0.5°$, 1200 torr Ar, and $I_1=I_2=0.5$ W/cm^2.)

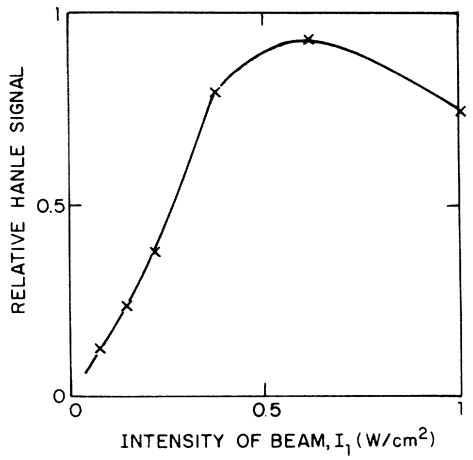

FIG. 15. Peak Hanle signal intensity vs intensity showing saturation in the strong pumping regime. ($\theta=0.3°$, $T_{oven}=185\,°C$, 1010 torr Ar, and $\Delta=0$ from D_1.)

low power was less than 10 percent exactly at the D_2 resonance. The width is due to residual Doppler broadening under the conditions of this experiment, $\theta=0.5°$, 1000 torr Ar pressure, and $I_1=0.5$ W/cm^2. It should be noted that the peak intensity for zero detuning at the D_1 resonance is about four times that of the D_2 resonance. The latter shows more pronounced wings. This linear plot cannot show in detail that the ratio $I(D_1)/I(D_2)$ indeed approaches unity for equal and large detuning. At this low Na vapor pressure the signal intensity in the wings is simply too weak. At larger detunings this vapor pressure may be increased, without running into optical-depth problems. In Fig. 14 the observed ratio $I(D_1)/I(D_2)$ for equal detuning Δ is plotted. For large Δ the weak-pumping regime prevails, and this ratio is indeed unity, as predicted both by the second perturbation theory of coherence and by the optical-pumping regime in this limit. As Δ is decreased, a transition to the strong-pumping regime occurs. The ratio of the intensities of the four-wave mixing approaches the limiting value 4, as the limiting

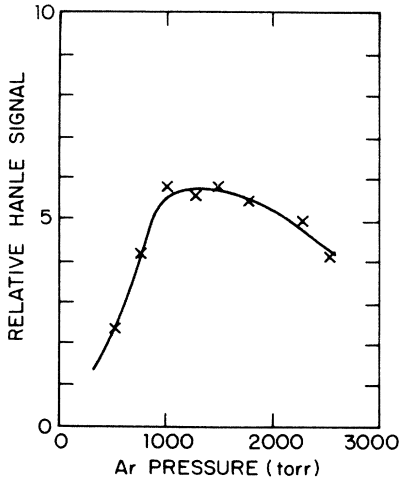

FIG. 16. Peak Hanle signal vs argon pressure showing saturation in the strong pumping regime. ($\theta=0.3°$, $T_{oven}=185\,°C$, $\Delta=20$ GHz below $^2P_{1/2}$, and $I_1=1$ W/cm^2.)

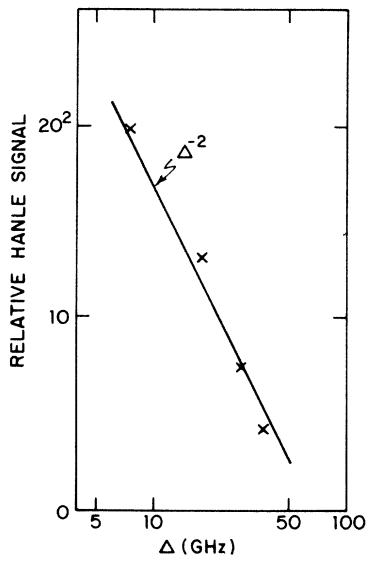

FIG. 17. Peak Hanle signal vs detuning in the strong pumping regime. ($\theta=0.4°$, $T_{oven}=175\,°C$, 1000 torr Ar, and $I_1=1$ W/cm^2.)

population-grating strength at the D_1 resonance is twice that at the D_2 resonance. This limiting value at smaller detuning is only obtained if the Na vapor pressure is lowered to avoid optical-depth problems. If the oven temperature is kept constant, this ratio increases to over twenty, as the D_2 signal intensity has relatively more attenuation.

The regime of strong optical pumping can also be reached at fixed detuning Δ, by raising the intensity of the incident beams or by raising the buffer-gas pressure, which increases Γ in Eqs. (3) and (8). As the population grating reaches its maximum value in the strong-pumping limit, the four-wave mixing signal should become independent of $|E_1|^2$, $|E_2|^2$, and p. Such saturation ef-

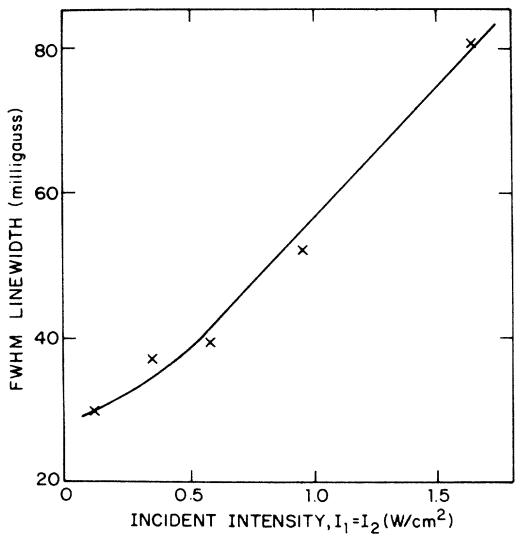

FIG. 18. The linewidth as a function of light intensity $I_1=I_2$. ($\theta=0.3°$, $T_{oven}=277\,°C$, $\Delta=50$ GHz below $^2P_{1/2}$, and 3050 torr Ar.)

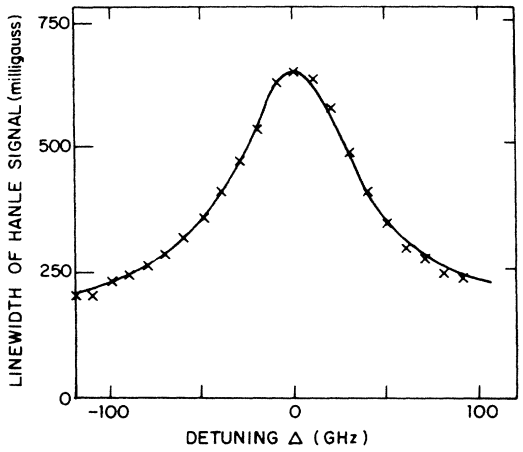

FIG. 19. Power-broadened linewidth with detuning Δ from D_2 line. ($\theta=0.8°$, $T_{\text{oven}}=265\,°\text{C}$, 4900 torr Ar, and $I_1=0.8$ W/cm^2.)

fects in the signal intensity have indeed been observed.

In these experiments the backward probing beam had an intensity of about 4% of the two forward beams of about equal intensity. The observed intensity of the four-wave Hanle signal exactly on the D_1 resonance $\Delta=0$, is plotted as a function of the intensity $|E_1|^2$ in Fig. 15. The data clearly show a saturation at power levels above about 0.5 W/cm^2. The exact interpretation is complicated by the fact that there is a nearly Gaussian distribution in the intensity $|E_1|^2$ and that the saturation first sets in at the extrema in the population grating, which consequently acquires a rather complex profile.

The saturation with buffer-gas pressure is revealed by the data in Fig. 16, which were taken at a constant detuning $\Delta=20$ GHz. The power level was high, $I_1=I_2=1$ W/cm^2. While peak intensity increases as p^3 or p^2 in the low-intensity regime, as confirmed by the data of Fig. 7, a saturation phenomenon, under the conditions listed, sets in at an argon pressure $p=1000$ torr. This saturation behavior must be carefully distinguished from a decrease in peak signal when the pressure-induced width Γ exceeds the detuning Δ. The factor $\Gamma/(\Delta^2+\Gamma^2)$ in Eq. (3) then changes from Γ/Δ^2 to Γ^{-1}. For $\Delta=20$ GHz, this effect should cause a maximum at $p=2500$ torr of argon. This maximum should be independent of the power level. The leveling off at $p=1000$ torr shown in Fig. 16 only occurs at high incident-beam intensity and is a saturation phenomenon.

In this regime the strength of the population grating should also become independent of the detuning Δ. Thus the only dependence on Δ should come from the probe-beam response function. As is evident from Eq. (8), this should change the detuning response from a Δ^{-6} dependence valid in the weak-pumping regime to a Δ^{-2} dependence in the strong-pumping regime. This is indeed confirmed by the data in Fig. 17, which were taken under experimental conditions of strong pumping.

The contribution of power broadening to the linewidth, given by Eq. (14), was also confirmed. The increase in linewidth as a function of $|E_1|^2=|E_2|^2$ is shown in Fig. 18, and the variation in the linewidth as a function of

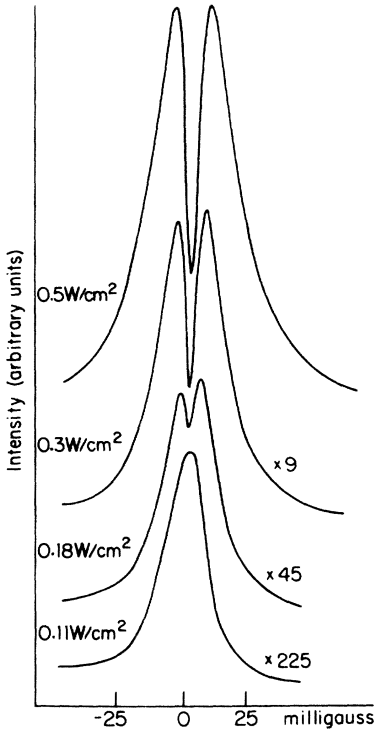

FIG. 20. Collision-enhanced Hanle resonances for various power flux densities in watts/cm^2 of the incident beams. ($\theta=0.3°$, $T_{\text{oven}}=310\,°\text{C}$, $\Delta=50$ GHz below $^2P_{1/2}$, and 1000 torr He.)

detuning Δ is shown in Fig. 19. This last figure shows very good agreement with a Lorentzian fit and represents an independent determination of the width Γ. From Eq. (14) and the known argon pressure, a cross section for Na-Ar collisions perturbing the p state is derived to be $\sigma=3.16\times10^{-14}$ cm^2. This is in agreement with earlier work on collisional broadening of the D_2 resonance line.[3]

The power broadening near the D_2 resonance is twice as large, because the pumping-out rate from the ground-state levels is twice as large for transitions to the $3\,^2P_{3/2}$ manifold. This is also evident from Fig. 8, when the sum of the square of the matrix elements, or of the Rabi frequencies, is taken. Experiments on the power broadening with tuning near the D_2 resonance confirmed this factor of 2.

VI. CONCLUSION

While the collision-assisted effects, on which this paper has primarily focused, are most evident for sufficiently large detuning Δ, an extensive body of theoretical and experimental work[27–29] in four-wave conjugate mixing has been published, in which the laser frequency is tuned inside the one-photon Doppler profile. In this case specific velocity packets are present for which $\Delta=0$. At relatively low buffer-gas pressures such packets are readily saturated, in the sense that a considerable fraction of the Na atoms is raised to the $3\,^2P$ states. In this case a new regime results, in which the inequality on the left-hand side of Eq. (13) is violated. Under these conditions a narrow dip in the center of the resonance has been predicted by

several theoretical papers.[27,28] When saturation is induced in the ground-state manifold by on-resonance light within the Doppler profile, it is also possible to obtain a saturation dip without appreciable P-state population, as discussed theoretically by Agrawal.[30] Köster *et al.*[31] have reported such line splittings in the four-wave mixing signal for the Hanle resonance in Na vapor.

We have also observed a center dip in the Hanle resonance, as shown in Fig. 20. This dip was, however, never observed on separate Zeeman components in a small external field B_0 (compare Fig. 2). The dip is only observed if the backward probe beam with wave vector ($\mathbf{k}_3$) is polarized in the z direction, but not if it is polarized in the y direction, perpendicular to B_0. The dip only appears at very high intensities, at which the inequality in Eq. (13) is violated. Further detailed theoretical investigations of this regime with significant $3\,^2P$-state population in the presence of appreciable detuning and strong collisions at high buffer-gas pressure are necessary.

The characteristics of the collision-enhanced Hanle resonances in four-wave mixing in the ground-state manifold of alkali vapor with high pressure of buffer gases are well understood. The collision-enhanced Zeeman or Hanle coherences are equivalent to collision-enhanced transverse optical pumping in the weak-pumping limit.

This description of the identical physical effect in two different frames of reference, which are simply related to each other by a 90° rotation of the axis of spatial quantization, has educational value and increases the insight into the nature of collision-assisted coherence.

The power broadening and saturation effects of collision-assisted Hanle resonances in four-wave mixing are also understood in the strong-pumping regime, as long as the build up of population in the excited electronic configuration may still be ignored. Collision-assisted effects of ground-state coherences in the presence of a sizable build up of populations in the excited configuration need further study.

ACKNOWLEDGMENTS

The assistance of and helpful discussions with Dr. Lewis Rothberg in the early phases of this work are gratefully acknowledged. This research was supported by the Joint Services Electronics Program of the U.S. Department of Defense under Contract No. N00014-84-K-0465.

---

*On leave from Peking University, Beijing, People's Republic of China.

[1]L. J. Rothberg and N. Bloembergen, Phys. Rev. A **30**, 820 (1984).

[2]N. Bloembergen, Y. H. Zou, and L. J. Rothberg, Phys. Rev. Lett. **54**, 186 (1985).

[3]E. L. Lewis, Phys. Rep. **58**, 1 (1980).

[4]A. T. Ramsey and L. W. Anderson, Nuovo Cimento **32**, 1151 (1964).

[5]W. Happer, Rev. Mod. Phys. **44**, 169 (1972).

[6]W. Happer and H. Tang, Phys. Rev. Lett. **31**, 273 (1973); W. Happer and A. C. Tam, Phys. Rev. A **16**, 1877 (1977).

[7]R. H. Dicke, Phys. Rev. **89**, 472 (1953).

[8]E. M. Purcell, R. V. Pound, and N. Bloembergen, Phys. Rev. **70**, 986 (1946).

[9]Y. Prior, A. R. Bogdan, M. Dagenais, and N. Bloembergen, Phys. Rev. Lett. **46**, 111 (1981).

[10]G. Grynberg, Opt. Commun. **38**, 439 (1981).

[11]R. Scholz, J. Mlynek, A. Gierulski, and W. Lange, Appl. Phys. B **28**, 191 (1982).

[12]R. Scholz, J. Mlynek, and W. Lange, Phys. Rev. Lett. **51**, 1761 (1983).

[13]G. Grynberg, J. de Phys. (Paris) B **14**, 2089 (1981).

[14]J. Szudy and W. E. Baylis, J. Quant. Spectrosc. Radiat. Transfer **15**, 641 (1975).

[15]S. Yeh and P. R. Berman, Phys. Rev. A **19**, 1106 (1979).

[16]Y. Prior and A. Ben-Reuven, Phys. Rev. A (to be published).

[17]See, for example, C. Cohen-Tannoudji, A. Kastler, in *Progress in Optics V*, edited by E. Wolf (Wiley, New York, 1966), p. 1.

[18]N. Bloembergen, in Proceedings of the "Symposium Kastler," Paris, 1985, edited by F. Laloe, Ann. Phys. (Paris) (to be published).

[19]W. Franzen and A. G. Emslie, Phys. Rev. **108**, 1453 (1957).

[20]H. G. Dehmelt, Phys. Rev. **105**, 1487 (1957).

[21]W. E. Bell and A. L. Bloom, Phys. Rev. Lett. **6**, 280 (1961).

[22]M. Ducloy and D. Bloch, Phys. Rev. A **30**, 3107 (1984).

[23]H. R. Gray, R. M. Whitley, and C. R. Stroud, Jr., Opt. Lett. **3**, 218 (1978).

[24]R. G. Brewer and E. L. Hahn, Phys. Rev. A **11**, 1641 (1975).

[25]See, for example, V. S. Letokhov, and V. P. Chebotayev, *Nonlinear Laser Spectroscopy* (Springer, Berlin, 1977).

[26]G. Orriols, Nuovo Cimento B **53**, 1 (1979).

[27]D. Bloch and M. Ducloy, J. Opt. Soc. Am. **73**, 635 (1983); **73**, 1844 (1983); Opt. Commun. **47**, 351 (1983); D. Bloch and M. Ducloy, Phys. Rev. A **30**, 3107 (1984).

[28]G. Grynberg, M. Pinard, and P. Verkerk, Opt. Commun. **50**, 261 (1984).

[29]J. F. Lam, D. G. Steel, and R. A. McFarlane, Phys. Rev. Lett. **49**, 1628 (1982); D. G. Steel and R. A. McFarlane, Phys. Rev. A **27**, 1217 (1983).

[30]G. P. Agrawal, Phys. Rev. A **28**, 2286 (1983).

[31]E. Köster, J. Mlynek, and W. Lange, Opt. Commun. **53**, 53 (1985).